JMEPEG
https://doi.org/10.1007/s11665-024-09343-4

1059-9495/$19.00

ORIGINAL RESEARCH ARTICLE

Experimental and Numerical Analysis of the Three-Point Bending Behavior of Hybrid Adhesive-Bonded Aluminum–Wood Plates

Eva Graf, Philipp Matz, Peter Auer, Christian Kurzböck, Thomas Krenke, Johannes Painer, Lukas Gruber, Michael Frieß, Christoph Bauer, Christof Sommitsch, and Josef Domitner

Submitted: 15 September 2023 / Revised: 3 January 2024 / Accepted: 15 February 2024

Hybrid components of wood-based materials offer a high potential for automotive lightweight applications. To investigate the bending behavior of hybrid aluminum-wood plates, commercial 1-mm-thick sheets of EN AW-6016-T4 aluminum alloy were adhesive-bonded with 4.2-mm-thick plates of birch wood. Orientations of the wood fibers parallel (longitudinal) as well as perpendicular (transverse) to the rolling direction of the aluminum alloy sheet and three different moisture contents of the wood plate were considered. The hybrid aluminum-wood plates were subjected to three-point bending at room temperature. Simple wood plates without aluminum alloy sheets were also tested. The bending force-bending angle curves monitored during bending, the bending angles at maximum bending force and the surface strains were evaluated. Moreover, a finite element model of the testing setup was created using the LS-Dyna software. The different moisture contents did not significantly influence the bending angle; however, moisture decreased the maximum bending force. Debonding was identified as critical failure mechanism. The FE model that considered the experimentally determined material properties was able to predict the bending behavior for different moisture conditions.

Keywords adhesive, aluminum alloy, automotive industry, bending behavior, finite element simulation, lightweight design, solid wood, wood–metal composites

1. Introduction

In recent years, the automotive industry has been facing growing challenges regarding the reduction of greenhouse gas emissions (Ref 1). According to Regulation (EU) 2021/1119, the CO_2 emissions of the European Union on the basis of 1990 should be reduced by 55 % until 2030, and the zero-emission policy aims for climate neutrality in 2050 (Ref 2). In particular, decreasing the vehicle weight in order to improve the fuel efficiency can substantially contribute to the achievement of these goals (Ref 3). Therefore, substituting conventional steels by lightweight materials such as high-strength steels (HSS), aluminum alloys, magnesium alloys and composites (e.g., carbon fiber-reinforced plastics, CFRP) has been in the main focus of vehicle manufacturers (Ref 4, 5). Because of the high strength-to-weight ratio and the good corrosion resistance, especially aluminum alloys of the 5000 and 6000 series are nowadays used in car bodies (Ref 6). Plastics and composites are of increasing interest, as they possess low densities and high strengths (Ref 5). Nevertheless, these materials have several disadvantages in terms of costs and energy consumption during production, and their recyclability is limited (Ref 7).

Wood as natural renewable resource does not have these issues. It is biodegradable, has a high specific strength that offers a great lightweight potential (the strength-to-weight ratios of wood, automotive steels and aluminum alloys are quite similar), and processing of wood with state-of-the-art technologies is straightforward and cost-efficient. However, wood has highly anisotropic properties. For example, the tensile strength transverse to the fiber orientation is only about 1/10 of the tensile strength in fiber orientation (Ref 8, 9).

During the last centuries, structural wood components have typically been used for building and construction applications (Ref 10, 11). For this reason, testing has focused on the bending behavior of comparatively large wood components. Uzel et al. (Ref 12) conducted four-point bending tests on glue-laminated (GLULAM) timber beams retrofitted with various types of nets on the lamination surfaces. They evaluated the results in terms of maximum load-bearing capacity and energy dissipation

This article is an invited submission to the Journal of Materials Engineering and Performance selected from presentations at the symposium "Joining," belonging to the area "Processing" at the 17th European Congress and Exhibition on Advanced Materials and Processes (EUROMAT 2023), held in Frankfurt am Main, Germany from September 3–7, 2023.

Eva Graf, Peter Auer, Christof Sommitsch, and **Josef Domitner**, Institute of Materials Science, Joining and Forming, Research Group of Lightweight and Forming Technologies, Graz University of Technology (TUG), Inffeldgasse 11/I, 8010 Graz, Austria; **Philipp Matz** and **Christian Kurzböck**, Virtual Vehicle Research GmbH (ViF), Inffeldgasse 21A, 8010 Graz, Austria; **Thomas Krenke, Johannes Painer,** and **Lukas Gruber**, Innovation Centre W.E.I.Z., W.E.I.Z. Forschungs & Entwicklungs gGmbH, Franz-Pichler-Straße 30, 8160 Weiz, Austria; and **Michael Frieß** and **Christoph Bauer**, Weitzer Woodsolutions GmbH, Klammstraße 24, 8160 Weiz, Austria. Contact e-mail: eva.graf@tugraz.at.

Published online: 01 April 2024

capacity and found out, that the nets notably increased the load-bearing capacity of the specimens. Several studies focused on the reinforcement of wooden structures by fiber-reinforced plastic (FRP) laminates, which can effectively increase the load-bearing capacity and the strength of timber beams (Ref 13-16). Nevertheless, research on metal reinforcements, especially on aluminum reinforcements, is still limited (Ref 17). Jasienko et al. (Ref 18) studied four-point bending of historic timber beams that were adhesive-bonded to steel plates. This measure significantly increased the load-bearing capacity of the beams; the capacity of the wood-steel hybrids was comparable with the capacity of FRP.

The accelerating trend toward CO_2-neutral sustainable solutions increases the interest on wood-based materials even for applications outside the classical field of civil engineering. During the early decades of the last century, wood-based structural components had already been used in automobiles and aircrafts (Ref 19, 20), until they were finally substituted by steel and aluminum alloy components. With regard to this former use, Baumann et al. (Ref 21) investigated the feasibility of using birch wood for crash-relevant automotive components at different temperatures, and Müller et al. (Ref 22) demonstrated that these components can fulfill the particular requirements under crash loading. Their research was focused on the mechanical properties such as load-bearing capacity and energy dissipation capacity of engineered wood products (EWP), but not on the processing (formability and joinability) of wood. Silvayeh et al. (Ref 23) and Domitner et al. (Ref 24) investigated hybrid screw-bonding of cross-laminated birch and beech plates with aluminum alloy sheets. They concluded that choosing the appropriate adhesive is crucial, as the adhesive provides the main contribution to the static and cyclic load-bearing capacities, but the screws contribute only little.

The inherent anisotropy and the considerable scattering of the mechanical properties makes the industrial serial production of wood components challenging, and quantifying the mechanical properties and the fracture behavior becomes difficult. The poor tensile ductility of dry wood at room temperature does not allow for multi-axial forming of complex-shaped components. Therefore, the Thonet forming procedure, also known as bentwood procedure, uses a metal strip for bearing the tensile stress during forming of wooden furniture products at elevated temperatures and moisture contents (Ref 25). In general, increasing either the moisture content (MC) or the temperature (T) tends to improve the tensile ductility and thus the formability of wood (Ref 26). However, increasing the MC just by 1 wt.% decreases the compressive strength by about 4-6 % and the tensile strength by about 1.5-3% (Ref 26-28).

Numerical simulations enable investigating the behavior of wood to identify failure mechanisms or potential design issues as demonstrated in the literature (Ref 29, 30, 31, 32, 33, 37). Baumann et al. (Ref 34) studied the suitability of material models that are available in the LS-Dyna finite element (FE) software for modeling birch wood. They successfully described the tensile characteristics of birch using the *MAT_58 model. Ivanov et al. (Ref 35) studied the behavior of plywood loaded in different directions by compact tension (CT) tests and modeling using the ABAQUS FE software. They qualitatively predicted the progressive failures occurring during CT testing. Mackenzie-Helnwein et al. (Ref 36, 37) created a constitutive model for studying the anisotropic inelastic behavior of biaxially loaded clear spruce wood using the MSC.marc 2003 software. Their model was able to predict failure locations and relevant failure modes.

Although previous studies have investigated the load-bearing capacity of solid wood components with and without different reinforcements in the construction sector, detailed studies on the forming behavior of hybrid metal-wood composites are quite rare. As (1) reinforcements may improve the load-bearing capacity of wood-based components and (2) external metal straps as used in the well-known Thonet process improve the bendability of solid wood, the present work combines both of these principles to achieve well-bendable adhesive-bonded metal-wood composites. Therefore, a finite element (FE) model that considers experimentally determined properties of an 6016 aluminum alloy (Ref 38) and of birch wood at different moisture conditions (Ref 39) was created for investigating the bending behavior of hybrid aluminum-wood plates. The results of the simulations were validated with three-point bending experiments. The numerical model enables predicting not only the structural response, but also the forming behavior of hybrid metal-wood composites, which opens the possibility for introducing wood into advanced applications such as car bodies.

2. Materials and Methods

2.1 Sample Preparation

For producing hybrid aluminum-wood plates, sheets of EN AW-6016-T4 aluminum alloy (250 mm × 60 mm × 1 mm) were glued with air-dried plates of birch wood (250 mm × 60 mm × 4.2 ± 0.1 mm) using 200-300 g/m^2 of commercial liquid single-component polyurethane-(PUR)-based adhesive. It was shown that the strength of PUR-bonded beech wood does not significantly decrease during short-term moisture exposure (Ref 40). The overall thickness of the hybrid plates (wood plate + adhesive layer + aluminum alloy sheet) was about 5.5 mm. The densities of the aluminum alloy sheet and of the air-dried birch wood plate were 2.7 g/cm^3 and about 0.7 g/cm^3, respectively. As schematically illustrated in Fig. 1, different orientations of the wood fibers were considered in this work. Until the adhesive was completely cured, the aluminum-wood compound was compressed with about 0.5 N/mm^2 for 4-5 h at room temperature using an OTT 3013 veneer panel press.

Three different conditions of the samples were considered at room temperature (20 °C):

- Air-dried/as-received (MC = 6.3-7.2 wt.%)
- Moistened (MC = 12.1-28.0 wt.%): 15 g water was applied on the free side of the wood plate. The residual water was wiped off after 45 min and the sample was immediately tested.
- Water-stored (MC = 17.3-43.5 wt.%): The samples were stored inside of a water bath for 2 h before testing. A moisture gradient over the sample thickness (outside wet, but inside comparatively dry) was achieved.

2.2 Determining the Moisture Content

The procedure proposed by the ÖNORM EN 13183-1 standard (Ref 41) was modified for determining the gradient of

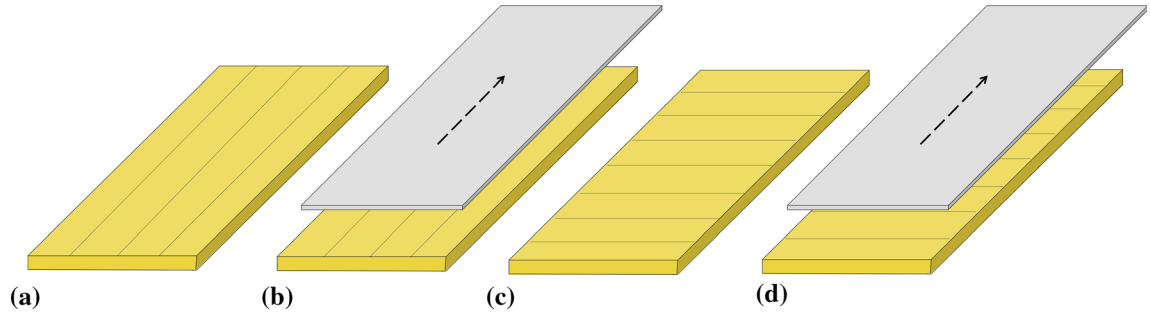

Fig. 1 Schematic illustration of (a, c) simple wood and (b, d) hybrid aluminum-wood plates; the arrow indicates the rolling direction of the aluminum alloy sheet, and the continuous lines indicate the fiber orientation of the wood plate. (a) Simple wood plate with longitudinal (L) fiber orientation, (b) hybrid aluminum-wood plate with wood fiber orientation parallel to the rolling direction of the aluminum alloy sheet, (c) simple wood plate with transverse (T) fiber orientation, and (d) hybrid aluminum-wood plate with wood fiber orientation transverse to the rolling direction of the aluminum alloy sheet

Fig. 2 Preparation of samples for determining the moisture content

the moisture content along the thickness of the wood plate. The sample thickness was divided into three sections, which were manually extracted by using a conventional chisel, as exemplarily demonstrated in Fig. 2. The initial mass m_0 of each extracted piece was weighed using a Kern PNS digital precision balance. The plates were heat-treated at the temperature of 100 ± 5 °C using a Siemens HT5HB33 oven, and after each hour of heating the actual mass m_1 of the extracted piece was measured. If m_1 decreased less than 2 mg within 2 h of heating, the wood was reasonably considered as dry and the moisture content MC in wt.% was calculated as $100(m_0 - m_1)/m_1$. The measured MC of each of the three sections over the sample thickness was used as input for the FE simulation of the bending process, as summarized in Table 1.

2.3 Three-Point Bending Tests

A Zwick/Roell Z100 uniaxial testing machine equipped with a 100-kN load cell was used for performing the three-point bending tests. The testing setup, the constraint conditions and the application of the bending load are schematically illustrated in Fig. 3. Testing was stopped when the maximum bending force that was continuously monitored during testing had decreased by 20 %. The testXpert III-V1.4 software was used for processing the measured data. The bending angle was

Table 1 Moisture contents in wt.% determined as input parameter for the FE simulation

Condition	Upper section	Center section	Lower section
Air-dried	7	7	7
Moistened	20	15	15
Water-stored	30	25	20

calculated based on VDA 238-100 (Ref 42), which considers the dimensions of the testing setup, the thickness of the sample and the measured punch displacement. Each of the sample types shown in Fig. 1 was three-times tested in the three conditions air-dried, moistened, and water-stored.

A plate that is exposed to three-point bending shows the greatest compressive stress on the inner bending radius (at the punch side) and the greatest tensile stress on the outer bending radius (at the support roll side). To bear the tensile stresses and thus to prevent tension-induced fracture of wood during bending, the aluminum alloy sheet of the hybrid aluminum-wood plate was placed at the outer bending radius, as schematically shown in Fig. 3(a). Locating the aluminum sheet of the hybrid aluminum-wood plate at the inner bend radius (i.e., at the punch side) would cause early macroscopic tensile fracture of wood.

The GOM ARAMIS 3D camera system with the measuring volume of 150 mm × 120 mm × 90 mm was used for optical measurements of the strains of selected air-dried samples based on digital image correlation (DIC) (Ref 43). For that purpose, the side face of the sample was sprayed with a white base coating followed by a pattern of stochastically distributed black speckles. The strain field on the surface of the sample was calculated based on the recorded displacements of the speckles during three-point bending using the GOM ARAMIS Professional 2018 software.

2.4 Three-Point Bending Simulation

The LS-Dyna R1310 FE software was used for modeling three-point bending of the hybrid aluminum-wood samples. As in the experiments, the overall dimensions of the modeled sample were 250 mm × 60 mm × 5.5 mm; the thickness of the wood plate and of the aluminum sheet was 4.5 and 1.0 mm, respectively. Moisture-induced swelling of the wood plate was

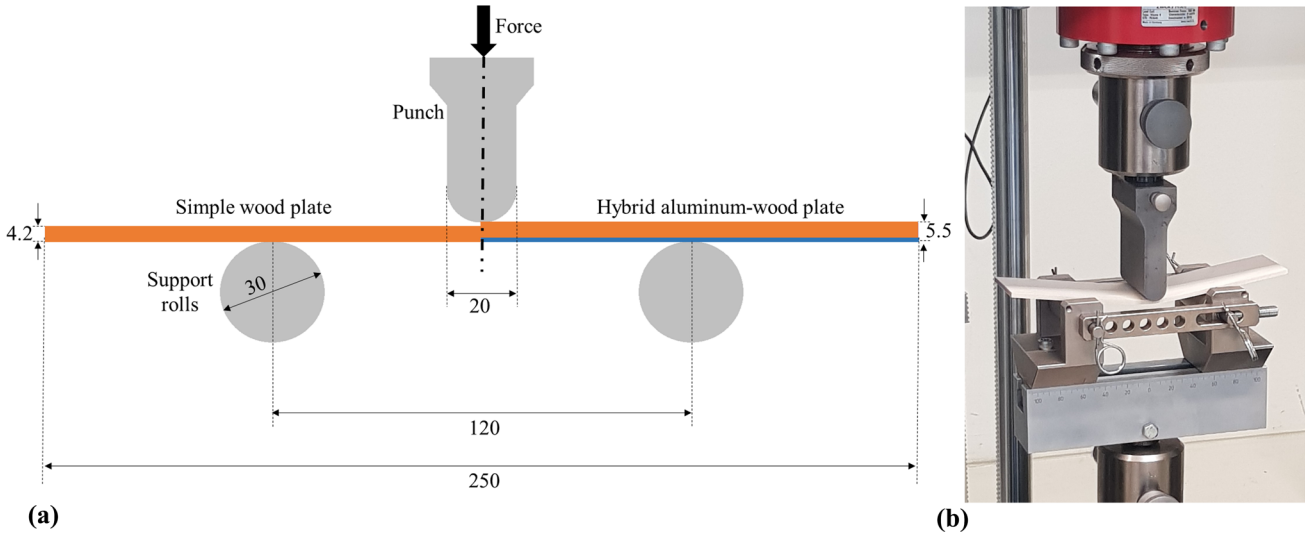

Fig. 3 (a) Schematic of simple wood plate testing (left half) and hybrid aluminum-wood plate testing (right half) with dimensions in mm, and (b) photo captured during one of the three-point bending tests showing the punch, the support rolls and a bent wood sample

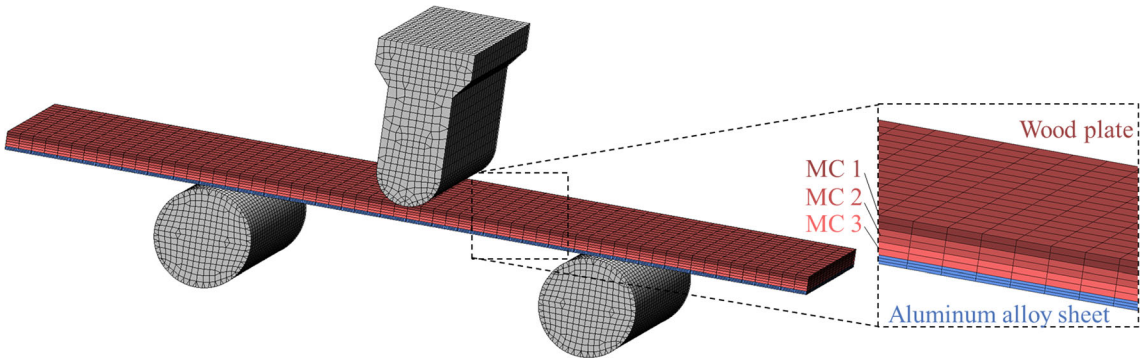

Fig. 4 Meshed FE model. The aluminum alloy sheet was meshed with three layers (blue) and the wood plate was meshed with six layers (red). Three different moisture contents as indicated by the dark red, medium red and light red mesh layers were considered over the thickness of the wood plate (Color figure online)

neglected. The model was meshed using solid elements (ELFORM = − 1) with dimensions of 4 mm × 4 mm × 0.75 mm and 4 mm × 4 mm × 0.33 mm for the wood plate and the aluminum sheet, respectively. The meshed model is illustrated in Fig. 4. Contacts between sample, support rolls and punch were considered using *CONTACT_AUTOMATIC_SURFACE_TO_SURFACE, and self-contact of the sample was considered using *CONTACT_AUTOMATIC_SINGLE_SURFACE. The calculated bending force-bending angle curves were filtered with the channel filter class (CFC) 60. The aluminum alloy was described using the MAT_PIECEWISE_LINEAR_PLASTICITY (MAT_24) material model, and the punch and the support rolls were described using the MAT_RIGID material model (Ref 44). The orthotropic behavior of wood was described using the MAT_58 material model, which considers quasi-brittle behavior in tension and ideal plastic behavior in compression. Its suitability for modeling wood was already proven (Ref 34). As the MC varies considerably over the thickness of the wood plate, the model had three different sections, each with particular MC. The properties of birch wood (Young's modulus, shear modulus, tensile strength, compressive strength (Ref 39) and shear strength) were defined depending on the MC. The adhesive layer was not explicitly modeled; however, a tied contact between the aluminum alloy sheet and the wood plate was considered. Possible debonding was neglected.

3. Results and Discussion

The bending force-bending angle curves recorded in the three-point bending tests for (a) air-dried, (b) moistened, and (c) water-stored conditions of the wood are shown in Fig. 5. Even at identical testing conditions the curves displayed for each of the four sample types differ considerably, which is attributed to the varying mechanical properties of the wood plates. However, the curves obtained in bending of simple aluminum alloy sheets are virtually identical, which is due to the constant mechanical properties of the sheets. The maximum bending force of the hybrid aluminum-wood plates with longitudinal and transverse fiber orientation was about 10-times and 2-times higher than the maximum bending force of the simple aluminum alloy sheets. Failure of the wood plate was initiated at the maximum bending force, and the bending force decreased as failure of the wood plate continued.

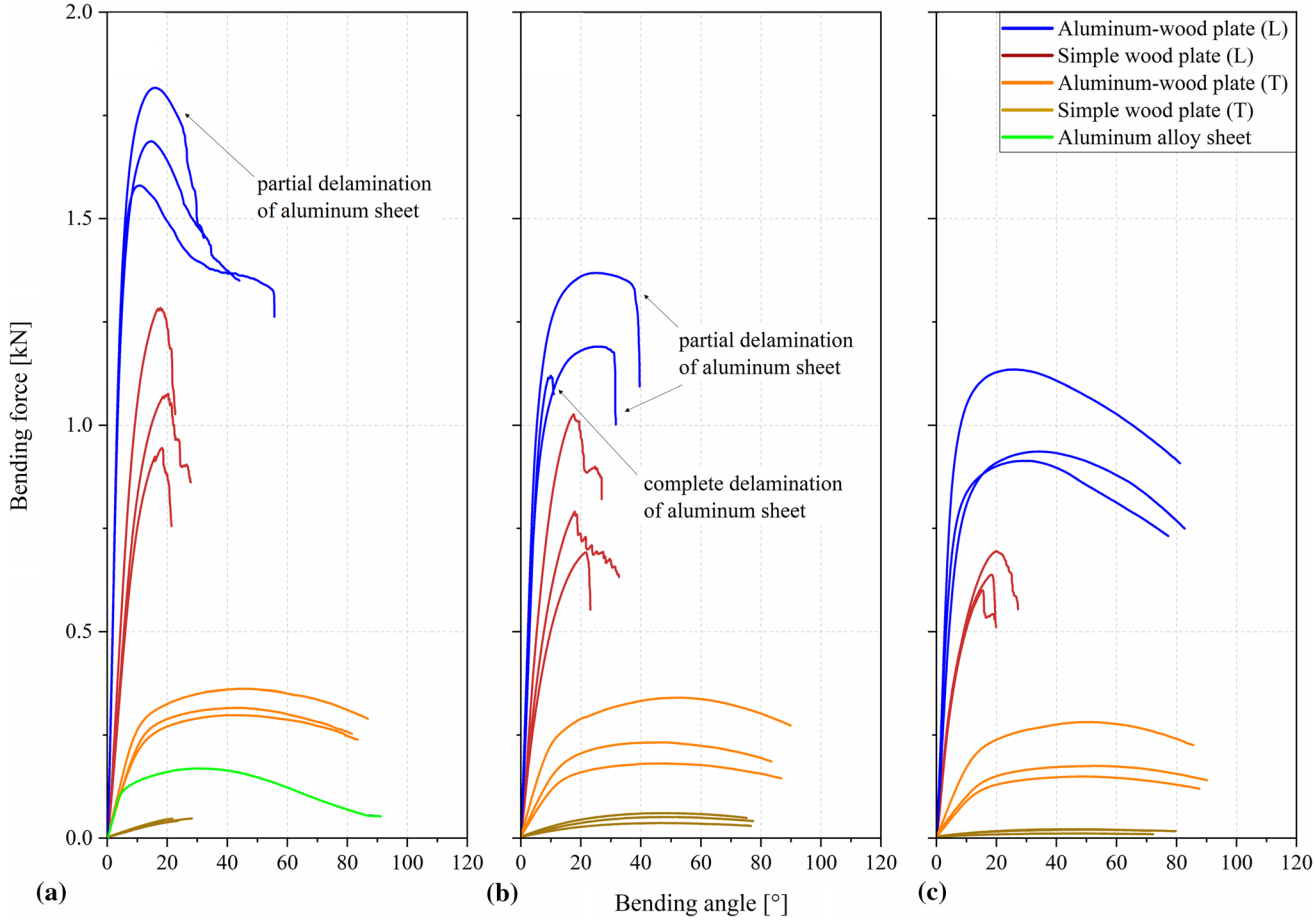

Fig. 5 Bending force-bending angle curves of tested samples with longitudinal (L) and transverse (T) fiber orientation in (a) air-dried, (b) moistened and (c) water-stored condition. The moisture content of the wood is increasing from left to right

The fracture mode of the wood plates was investigated at macroscopic scale. Nevertheless, microscopic fracture of the wood fibers may even occur in early stages of deformation, which may affect the behavior of the wood component. Fracture of the aluminum sheet did not occur in any of the three-point bending tests. Nevertheless, in some cases debonding/delamination of the aluminum sheet occurred at the bending zone, as indicated by the abrupt decrease in the bending force after reaching its maximum. Delamination decreased the bending angle. Additionally, Fig. 5(a) illustrates the bending behavior of the 1 mm-thick aluminum alloy sheet. It is evident that the force for bending the hybrid aluminum-wood plate was generally higher than the force for bending the simple wood plate or the simple aluminum alloy sheet, respectively.

3.1 Influence of Fiber Orientation

In general, wood plates with longitudinal fiber orientation show higher bending forces than wood plates with transverse fiber orientation. For example, for MC = 12-15 wt.% the tensile strength of wood transverse to the fibers is only about 1/10 of the strength parallel to the fibers (Ref 9), and the compressive strength of birch wood transverse to the fibers is about 1/8 of the strength parallel to the fibers (Ref 8). Wang et al. (Ref 45) demonstrated, that birch plywood beams with longitudinal fiber orientation showed highest bending strength and Young's modulus, which agrees well with the results of this study.

3.1.1 Longitudinal Fiber Orientation. Consecutive fiber-by-fiber fracture occurred at the tension zone at the outer bending radius of simple wood plates, if the wood fibers were oriented in longitudinal direction. As illustrated in Fig. 4, this caused the stepwise decrease in the bending force after the maximum force had been reached. Even though the MC influenced the bending behavior, this influence was rather negligible for the fracture behavior of simple wood plates, as shown in Fig. 6(a), (c). In contrast, fracture of the hybrid aluminum-wood plate started at the compression zone of the inner bending radius. As exemplarily shown in Fig. 6(b), (d), local buckling of the wood fibers caused by compressive stresses was observed next to the punch. This kind of buckling failure at the compression zone was reduced in the water-stored condition. This behavior was basically confirmed by Sulzberger (Ref 46), who performed tensile and compression tests on hoop pine plywood at different MC and temperatures. He found that the influence on the tensile strength was less significant than the influence on the compressive strength, when the MC at the temperature of 20 °C increased from 8 to 20 wt.%. Figure 6(b) exemplarily shows debonding/delamination of the aluminum sheet from the wood plate at the bending zone. Debonding/delamination reduces the achievable bending angle. The macroscopic examination of the bonding interface revealed an adhesive fracture pattern on the aluminum interface, which typically indicates insufficient bonding (Ref 24, 47).

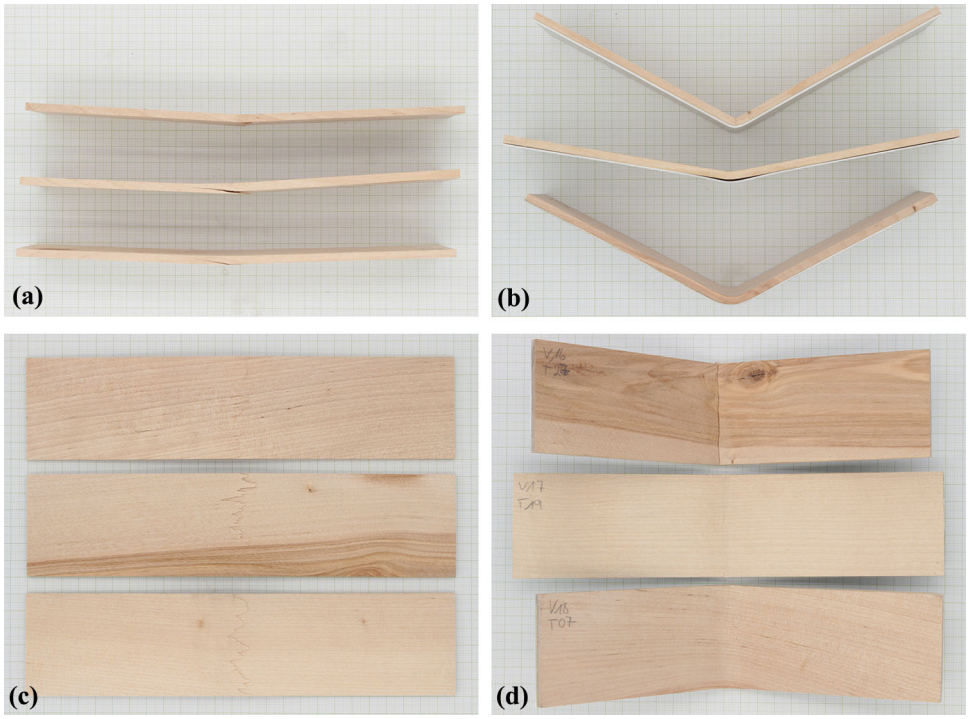

Fig. 6 (a, c) Simple wood plates (side view and view from below) and (b, d) hybrid aluminum-wood plates (side view and top view) with longitudinal fiber orientation. The upper, middle and bottom sample demonstrates the air-dried, moistened and water-stored condition after three-point bending, respectively

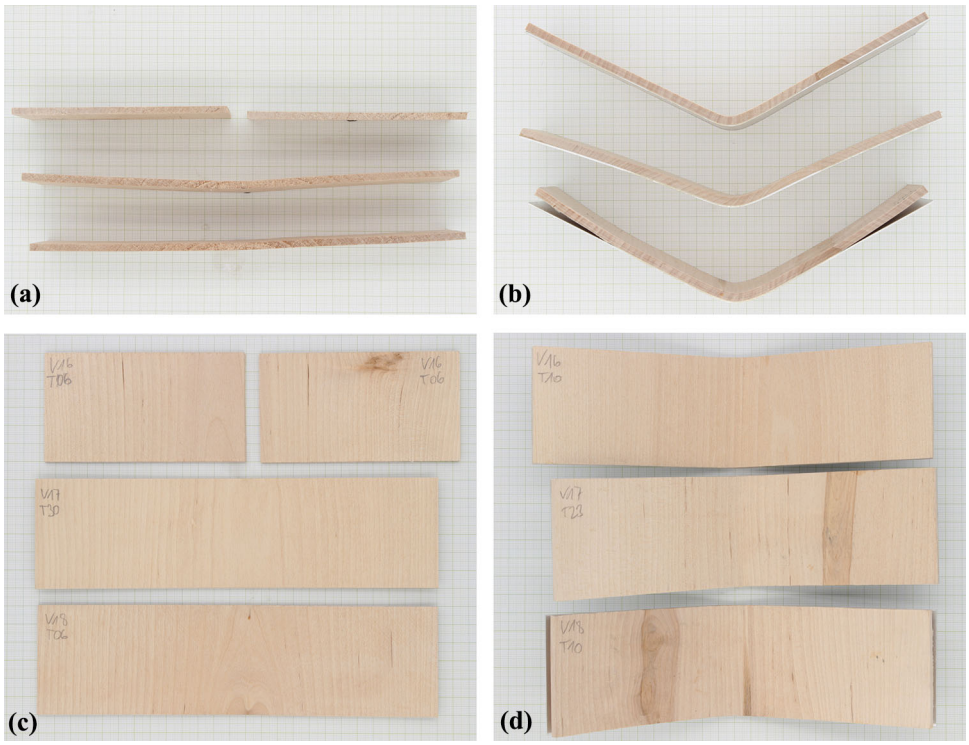

Fig. 7 (a, c) Simple wood plates (side view and top view) and (b, d) hybrid aluminum-wood plates (side view and top view) with transverse fiber orientation. Upper, middle and lower samples represent air-dried, moistened and water-stored conditions after three-point bending, respectively

3.1.2 Transverse Fiber Orientation. Brittle interfiber fracture occurs, if wood is loaded transverse to its fiber orientation. Figures 5 and 7(a), (c) demonstrate, that this fracture mode in simple wood plates was notably dependent on the moisture content (MC). The fracture strain of air-dried wood is comparatively small, Fig. 5(a), as indicated by the comparatively small bending angle. With increasing MC, the fracture strain and thus the bending angle increased. For moistened wood and for water-stored wood, Fig. 7(a), (c), macroscopic fracture was not observed. This brittle-to-ductile behavior is attributed to the change of the molecular bonding forces and of the characteristic microstructure of wood with increasing moisture content (Ref 10, 26, 45, 48, 49). Panshin and de Zeeuw (Ref 50) showed for clear wood the decrease in the Young's modulus and the modulus of rupture (MOR) with increasing MC.

As illustrated in Fig. 7(b), (d), even in air-dried condition the hybrid aluminum-wood plate did not show any macroscopic fracture at the bending zone. However, in water-stored condition debonding/delamination of the aluminum sheet from the wood plate occurred at the outer zones, but not directly at the bending zone. Additional stresses caused by swelling of wet wood may likely impact adhesive bonding (Ref 8). Hence, failure of the hybrid plates is rather caused by deboning/delamination of the aluminum sheet from the wood plate at the interface region than by deterioration of the mechanical properties of the adhesive itself (Ref 51).

Comparing the hybrid aluminum-wood plates with different fiber orientations, Figs. 6(b) and 7(b), generally reveals a sharper bending radius for wood with longitudinal fiber orientation.

3.2 Influence of Moisture Content (MC)

Figure 8 illustrates the dependence of the maximum bending force and of the bending angle that was measured at the maximum bending force from the MC of the wood plate. The MC was measured on reference samples and the average MC was considered as 7, 17 and 25 wt.% for air-dried, moistened and water-stored condition, respectively. With increasing MC, the bending force tended to decrease linearly for each of the four sample types, as the molecular bonding forces decrease with water application (Ref 10, 49). This confirms that the MC considerably influences the mechanical properties and, particularly, on the bending behavior of wood. Although the impact on the bending force was significant, the influence on the bending angle at maximum bending force was just moderate, except for the wood plate with transverse fiber orientation, because the aluminum alloy sheet prevented early interfiber fracture of the wood plate. However, for some of the hybrid aluminum-wood plates the bending angle was limited by delamination/debonding between the wood plate and the aluminum alloy sheet in the bending zone, as demonstrated in Fig. 6 (b). Debonding of the hybrid aluminum-wood plates at the early stage of bending was followed by the fracture behavior that was identical to the fracture behavior of simple wood plates. Therefore, reliable adhesive bonding was of utmost importance for achieving great bending angles and thus good formability of the aluminum-wood plates. Especially for simple wood plates and for hybrid aluminum-wood plates with longitudinal fiber orientation the bending force varies considerably, because wood characteristics like knots and high fiber angle deviations have significant influence on the mechanical properties and, thus, on the bending behavior. Moreover, debonding/delamination of hybrid aluminum-wood plates with longitudinal fiber orientation causes variations of the maximum bending forces.

3.3 Bending Simulation

Figure 9 compares the bending force-bending angle curves of the experiment and the FE simulation. Basically, good agreement was achieved for the hybrid aluminum-wood plates, but in longitudinal fiber orientation the difference increases with increasing moisture content. This could be attributed to the natural characteristics of wood (e.g., knots, fiber misorientations, variation of the MC), which may influence the mechanical properties (Ref 8), but which are not fully considered in the model. Fiber angle deviation may occur more frequently in samples with longitudinal fiber orientation than in samples with

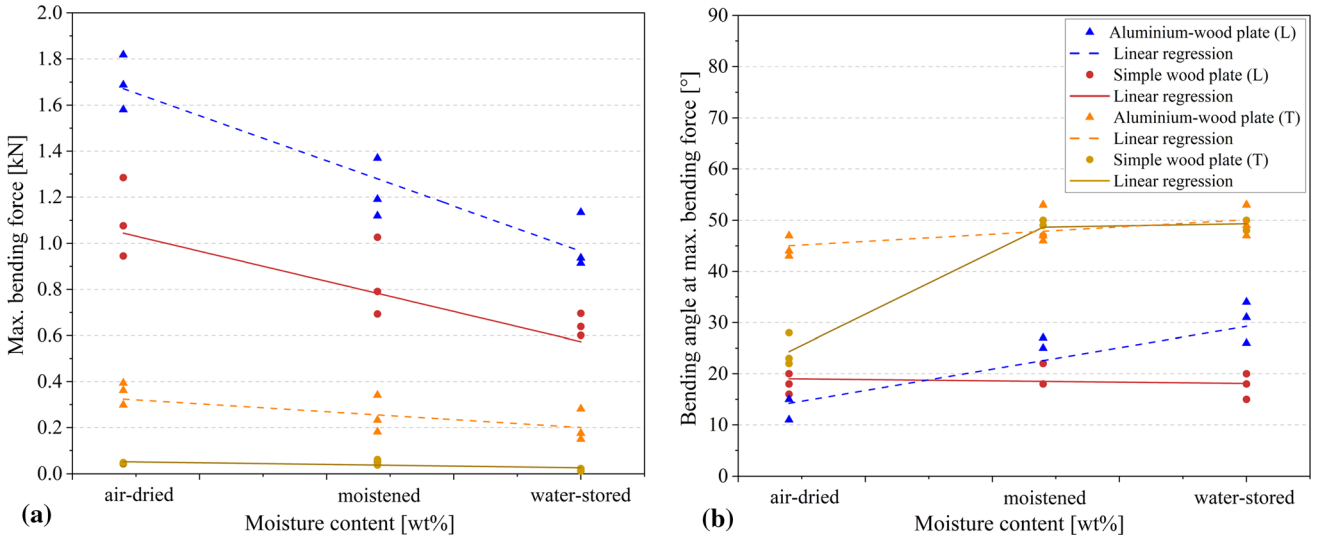

Fig. 8 (a) Maximum bending force and (b) bending angle at maximum bending force over the moisture content of wood plates with longitudinal (L) and transverse (T) fiber orientations. Samples showing complete delamination/debonding were not considered for calculating the bending angle

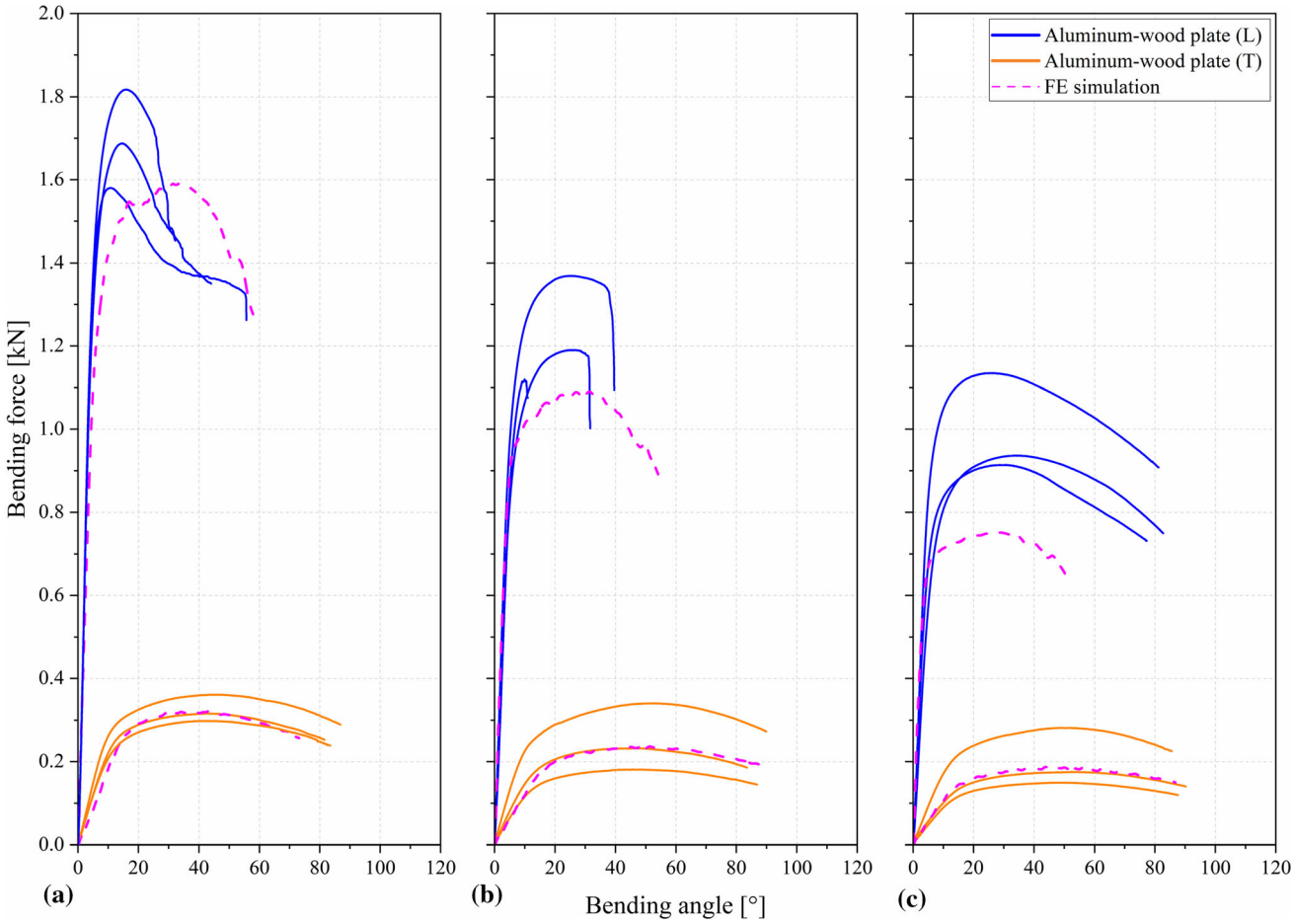

Fig. 9 Bending force-bending angle curves of hybrid aluminum-wood samples in (a) air-dried, (b) moistened and (c) water-stored condition. The moisture content of wood increases from left to right

transverse fiber orientation. The MC that was used as input for the FE model was solely determined on reference samples and it was considered identical for both fiber orientations as given in Table 1.

In general, higher bending angles can obviously be achieved, if hybrid metal-wood components do not debond/delaminate during bending. Thus, the importance of an appropriate adhesive that enables good bonding between aluminum and wood is crucial. However, as the presented simulation model does neither consider any mechanical properties nor any failure parameters of the adhesive, it does not allow for quantifying the actual contribution of the bonding interface to the bending behavior. Therefore, further improvement of the model is required.

As illustrated in Fig. 10, strain fields at the maximum bending angles of 44° and 83° were recorded on the surface of selected hybrid aluminum-wood plates with longitudinal and transverse fiber orientation, respectively. Zones of tensile strain (red) are observed at the outer bending radius and zones of compressive strain (blue) are detected at the inner bending radius. The tensile strain in the hybrid aluminum-wood plate with longitudinal fiber orientation (i.e., the major stresses are parallel to the fibers) was localized at the vertex of the outer bending radius; whereas, the tensile strain of the hybrid aluminum-wood plate with transverse fiber orientation (i.e., the main stresses are transverse to the fibers) was distributed more evenly over the outer bending radius. Therefore, only hybrid plates with longitudinal fiber orientation showed localized debonding/delamination at the heavily strained zone. It is evident that the compressive strain concentrates at the inner bending radius of the hybrid aluminum-wood plate with transverse fiber orientation. Hence, wood can be highly densified by plastic deformation above the proportionality limit, if it is exposed to compressive loading transverse to the fiber orientation (Ref 26).

4. Summary and Conclusions

This work investigates the bending behavior of simple wood and hybrid aluminum-wood plates at different moisture contents (MC) using three-point bending tests. A finite element (FE) model of the bending tests including experimentally determined properties of the aluminum alloy sheet and of the birch wood plate was created. Based on the results of the bending experiments and simulations, the following conclusions can be drawn:

- Increasing the MC of the wood plate generally tends to decrease the bending force, but the influence of the moisture content on the bending angle at maximum bending force is rather moderate. Only the bending angle of the simple wood plate with transverse fiber orientation in-

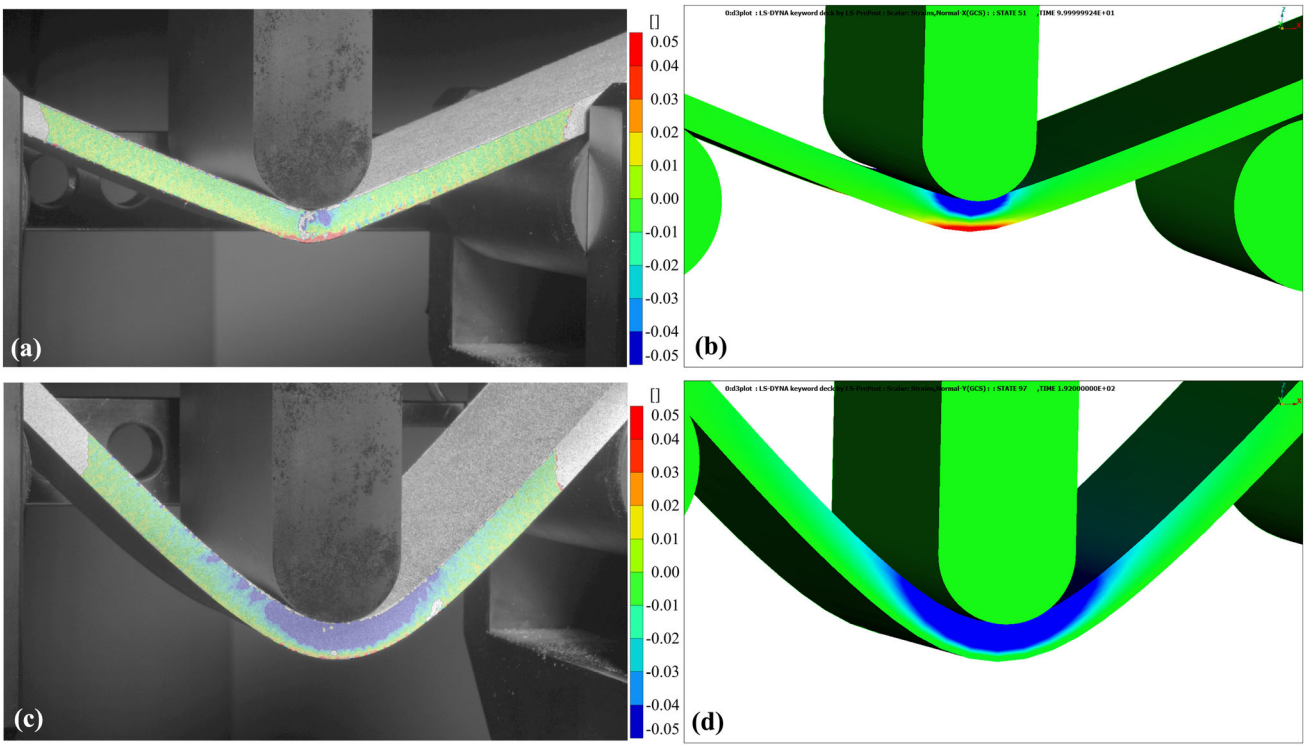

Fig. 10 Comparison of strain fields determined by (a, c) optical measurement and by (b, d) FE simulation at the maximum bending angle of hybrid aluminum-wood plates in air-dried condition for (a, b) the wood plate with longitudinal fiber orientation and (c, d) the wood plate with transverse fiber orientation. Positive and negative values illustrate tensile zones (red) and compressive zones (blue), respectively (Color figure online)

creases notably with increasing MC, since early interfiber fracture is prevented. Best bendability in terms of low punch force and great bending angle is achieved for hybrid aluminum-wood plates consisting of wood with transverse fiber orientation and increased MC.

- The bending angles of hybrid aluminum-wood plates are tendentially greater than the bending angles of simple wood plates, as the aluminum alloy sheet is able to bear tensile stresses that are particularly critical for wood in air-dried condition. However, debonding/delamination of the aluminum alloy sheet from the wood plate must be prevented.
- Debonding/delamination was identified as critical fracture mode that limits the bendability of hybrid aluminum-wood plates. Hence, reliable adhesive bonding is of utmost importance for achieving great bending angles and thus for obtaining good formability of hybrid aluminum-wood plates. At the outer bending radius greater local tensile strain was observed for plates with longitudinal wood fiber orientation than for plates with transverse wood fiber orientation, which may promote local adhesive failure.
- Because of the strong anisotropy and the scatter of the mechanical properties of wood the numerical simulation of wood forming processes is challenging. However, the created FE model was basically able to predict the bending force-bending angle curves and the surface strains of hybrid aluminum-wood plates in air-dried condition, although the differences to the experimental results increased with increasing MC.
- As the presented simulation model does neither consider any mechanical properties nor any failure parameters of the adhesive between the wood plate and the aluminum sheet, the actual contribution of the bonding interface to the bending behavior of the hybrid plates cannot be quantified. Therefore, improving the model by including adhesive properties as well as wood fiber misorientations is an ongoing work.

Author Contribution

Eva Graf contributed to conceptualization, formal analysis, visualization, investigation, validation, and writing—original & Draft. Philipp Matz contributed to conceptualization, software, and formal analysis; Validation Peter Auer contributed to conceptualization and methodology. Christian Kurzböck contributed to software. Thomas Krenke contributed to project administration. Johannes Painer contributed to Resources. Lukas Gruber contributed to resources. Michael Friess contributed to resources. Christoph Bauer contributed to resources. Christof Sommitsch contributed to supervision. Josef Domitner contributed to writing—review & editing, and supervision

Funding

Open access funding provided by Graz University of Technology. This study was part of the "Modelling, Production and Further Processing of Eco-Hybrid Structures and Materials" (CARpenTiER) project funded by the Austrian Federal Ministries of Climate Action, Environment, Energy, Mobility, Innovation and Technology (BMK) and of Labor and Economy (BMAW), by the

Province of Styria, and by partner companies within the Competence Centers for Excellent Technologies (COMET) program, which is processed by the Austrian Research Promotion Agency (FFG) and by the Styrian Business Promotion Agency (SFG).

Data Availability

The data that support the findings of this study are available from the corresponding author upon reasonable request.

Conflict of interest

The authors declare no conflict of interest.

Open Access

References

1. Regulation (EU) 2019/631 of the European Parliament and of the Council of 17 April 2019 Setting CO2 Emission Performance Standards for New Passenger Cars and for New Light Commercial Vehicles, and Repealing Regulations (EC) No 443/2009 and (EU) No 510/201. Official Journal of the European Union, The European Parliament and the Council of the European Union, 2019. Available online: https://eur-lex.europa.eu/legal-content/EN/TXT/PDF/?uri=CELEX:32019R0631&from=EN (accessed 2023-06-23)
2. Regulation (EU) 2021/1119 of the European Parliament and of the Council of 30 June 2021 establishing the framework for achieving climate neutrality and amending Regulations (EC) No 401/2009 and (EU) 2018/1999 ('European Climate Law'). Official Journal of the European Union, The European Parliament and the Council of the European Union, 2021. Available online: https://eur-lex.europa.eu/legal-content/EN/TXT/?uri=CELEX:32021R1119 (accessed 2023-07-11)
3. G.P. Chirinda and S. Matope, The lighter the better: Weight reduction in the automotive industry and its impact on fuel consumption and climate change. In *Proceedings of the 2nd African. International Conference on Industrial Engineering and Operations Management*, Dec 7-10, 2020 (Harare, Zimbabwe), p 520–533
4. W. Zhang and J. Xu, Advanced Lightweight Materials for Automobiles: A review, *Mater. Des.*, 2022, **221**, p 110994. https://doi.org/10.1016/j.matdes.2022.110994
5. M.A. Fentahun and M.A. Savas, Materials Used in Automotive Manufacture and Material Selection Using Ashby Charts, *Int. J. Mater. Eng.*, 2018, **8**(3), p 40–54. https://doi.org/10.5923/j.ijme.20180803.02
6. W.S. Miller, L. Zhuan, J. Bottema, A.J. Wittebrood, P. De Smet, A. Haszler and A. Vieregge, Recent Development in Aluminium Alloys for the Automotive Industry, *Mater. Sci. Eng. A*, 2000, **280**, p 37–49. https://doi.org/10.1016/S0921-5093(99)00653-X
7. D. Kohl, P. Link, and S. Böhm, Wood as a Technical Material for Structural Vehicle Components, *Procedia CIRP*, 2016, **40**, p 557–561. https://doi.org/10.1016/j.procir.2016.01.133
8. R. Ross, *Wood Handbook: Wood as an Engineering Material*, Centennial ed.; U.S. Department of Agriculture Forest Service, Forest Service, Forest Products Laboratory (FPL), Madison, WI, USA, 2010. https://doi.org/10.2737/FPL-GTR-190
9. R. Wagenführ and A. Wagenführ, *Holzatlas*, 7th ed. Carl Hanser Verlag, München, 2022, p 152–153, ISBN 978-344-646-838-2 (in German)
10. S. Thelandersson and H.J. Larsen, *Timber Engineering*, 1st ed. John Wiley & Sons Ltd, West Sussex, 2003, ISBN 978-047-084-469-4
11. J.J. Stalnaker and E.C. Harris, *Structural Design in Wood*, 1st ed. Springer, New York, 2013, p 11–12, ISBN 978-146-849-996-4
12. M. Uzel, A. Togay, Ö. Anil, and C. Söğütlü, Experimental Investigation of Flexural Behavior of Glulam Beams Reinforced with Different Bonding Surface Materials, *Constr. Build. Mater.*, 2018, **158**, p 149–163. https://doi.org/10.1016/j.conbuildmat.2017.10.033
13. Ü. Karagöz and H. Kesik, Experimental and Numerical Analysis of Compression and Bending Strength of Old Wood Reinforced with CFRP Strips, *Structures*, 2021, **33**, p 259–271. https://doi.org/10.1016/j.istruc.2021.04.070
14. A. Borri, M. Corradi, and A. Grazini, A Method for Flexural Reinforcement of Old Wood Beams with CFRP Materials, *Compos. Part B*, 2005, **36**(2), p 143–153. https://doi.org/10.1016/j.compositesb.2004.04.013
15. B. Wang, E.V. Bachtiar, L. Yan, B. Kasal, and V. Fiore, Flax, Basalt, E-Glass FRP and Their Hybrid FRP Strengthened Wood Beams: An Experimental Study, *Polymers*, 2019, **11**(8), p 1255. https://doi.org/10.3390/polym11081255
16. H. Alhayek and D. Svecova, Flexural Stiffness and Strength of GFRP-Reinforced Timber Beams, *J. Compos. Constr.*, 2012, **16**(3), p 245–252. https://doi.org/10.1061/(asce)cc.1943-5614.0000261
17. G. Fajdiga, B. Šubic, and A. Kovačič, Bending Stiffness of Hybrid Wood-Metal Composite Beams: An Experimentally Validated Numerical Model, *Forests*, 2021, **12**(7), p 918. https://doi.org/10.3390/f12070918
18. J. Jasieńko, and T.P. Nowak, Solid Timber Beams Strengthened with Steel Plates—Experimental Studies, *Constr. Build. Mater.*, 2014, **63**, p 81–88. https://doi.org/10.1016/j.conbuildmat.2014.04.020
19. E. Schatzberg, Ideology and Technical Choice: The Decline of the Wooden Airplane in the United States 1920–1945, *Technol. Cult.*, 1994, **35**(1), p 34–69
20. A.T. Upson and L.N. Ericksen, Wood for Automobile Bodies, *SAE Trans.*, 1924, **19**, p 513–531
21. G. Baumann, R. Brandner, U. Müller, C. Kumpenza, A. Stadlmann, and F. Feist, Temperature-Related Properties of Solid Birch Wood Under Quasi-Static and Dynamic Bending, *Materials*, 2020, **13**(23), p 5518. https://doi.org/10.3390/ma13235518
22. U. Müller, T. Jost, C. Kurzböck, A. Stadlmann, W. Wagner, S. Kirschbichler, G. Baumann, F. Feist, and M. Pramreiter, Crash Simulation of Wood and Composite Wood for Future Automotive Engineering, *Wood Mater. Sci. Eng.*, 2020, **15**(5), p 312–324. https://doi.org/10.1080/17480272.2019.1665581
23. Z. Silvayeh, J. Domitner, J. Predan, P. Auer, E. Graf, L. Ferlič, T. Krenke, C. Sommitsch and N. Gubeljak, Mechanical Performance of Hybrid Joints of Aluminum Sheets and Laminated Beech Veneer Plates: An Experimental Prestudy, *Procedia Struct. Integr.*, 2023, **51**, p 141–144. https://doi.org/10.1016/j.prostr.2023.10.080
24. J. Domitner, Z. Silvayeh, J. Predan, E. Graf, T. Krenke, and N. Gubeljak, Mechanical Performance and Failure Behavior of Screw-Bonded Joints of Aluminum Sheets and Cross-Laminated Birch Veneer Plates, *Eng. Fail. Anal.*, 2023, **146**, p 107074. https://doi.org/10.1016/j.engfailanal.2023.107074
25. P. Niemz, A. Teischinger, and D. Sandberg, *Springer Handbook of Wood Science and Technology*, Springer, Cham, 2023, p 945–953, ISBN 978-3-030-81315-4
26. P. Niemz and W.U. Sonderegger, *Holzphysik, Eigenschaften, Prüfung und Kennwerte*, 2nd ed. Carl Hanser Verlag, München, 2021, ISBN 978-344-647-010-1 (in German)
27. F. F. P. Kollmann, Technologie des Holzes und der Holzwerkstoffe. Erster Band. Anatomie und Pathologie, Chemie, Physik, Elastizität und Festigkeit, 2nd ed., Springer-Verlag, Berlin Heidelberg, Germany, 1951, p 663, ISBN 978-3-642-49474-1 (in German)
28. C. Skaar, *Wood-Water Relations*, 1st ed. Springer, Berlin, 1988, ISBN 978-364-273-683-4
29. Å. Bolmsvik, A. Linderholt, A. Brandt, and T. Ekevid, FE Modelling of Light Weight Wooden Assemblies—Parameter Study and Compar-

ison Between Analyses and Experiments, *Eng. Struct.*, 2014, **73**, p 125–142. https://doi.org/10.1016/j.engstruct.2014.04.028
30. M. Oudjene and M. Khelifa, Finite Element Modelling of Wooden Structures at Large Deformations and Brittle Failure Prediction, *Mater. Des.*, 2009, **30**(10), p 4081–4087. https://doi.org/10.1016/j.matdes.2009.05.024
31. D. Hoffmeyer and A.R. Damanpack, Bending and Torsion Induced Stresses in Cylindrically Orthotropic and Inhomogeneous Timber Beams, *Finite Elem. Anal. Des.*, 2024, **229**, p 104072. https://doi.org/10.1016/j.finel.2023.104072
32. F. Mirianon, S. Fortino, and T. Toratti, A method to model wood by using ABAQUS finite element software Part 1. Constitutive model and computational ABAQUS details, VTT Technical Research Centre of Finland, Finland, 2008, ISSN 1455-0849
33. M. Gaff, M. Gašparík, V. Borůvka, and M. Babiak, Simulating Stresses Associated with the Bending of Wood Using a Finite Element Method, *BioResources*, 2015, **10**(2), p 2009–2019. https://doi.org/10.15376/biores.10.2.2009-2019
34. G. Baumann, S. Hartmann, U. Müller, C. Kurzböck, F. Feist, Comparison of the two material models 58, 143 in LS Dyna for modelling solid birch wood. In Proceedings of the 12th European LS-DYNA Conference, May 14-16, 2019 (Koblenz, Germany)
35. I.V. Ivanov and T. Sadowski, Numerical Modelling and Investigation of Plywood Progressive Failure in CT Tests, *Comput. Mater. Sci.*, 2009, **45**(3), p 729–734. https://doi.org/10.1016/j.commatsci.2008.08.016
36. P. Mackenzie-Helnwein, H.W. Müllner, J. Eberhardsteiner, and H.A. Mang, Analysis of Layered Wooden Shells Using an Orthotropic Elasto-Plastic Model for Multi-axial Loading of Clear Spruce Wood, *Comput. Methods Appl. Mech. Eng.*, 2005, **194**(21–24), p 2661–2685. https://doi.org/10.1016/j.cma.2004.07.051
37. P. Mackenzie-Helnwein, J. Eberhardsteiner, and H.A. Mang, A Multi-surface Plasticity Model for Clear Wood and Its Application to the Finite Element Analysis of Structural Details, *Comput. Mech.*, 2003, **31**, p 204–218. https://doi.org/10.1007/s00466-003-0423-6
38. E. Hodžić, J. Domitner, A. Thum, A. Shafiee Sabet, N. Müllner, W. Fragner, and C. Sommitsch, Influence of Natural Aging on the Formability of Al-Mg-Si Alloy Blanks, *J. Manuf. Process.*, 2023, **94**, p 109–121. https://doi.org/10.1016/j.jmapro.2023.03.021
39. H. Al-musawi, C. Huber, M. Grabner, B. Ungerer, T. Krenke, P. Matz, A. Teischinger, and U. Müller, Compressive Strength of Beech and Birch at Different Moisture Contents and Temperature, *J. Mater. Sci.*, 2023 https://doi.org/10.1007/s10853-023-08882-w
40. J. Bomba, P. Šedivka, M. Böhm, and M. Devera, Influence of Moisture Content on the Bond Strength and Water Resistance of Bonded Wood Joints, *BioResources*, 2014, **9**(3), p 5208–5218. https://doi.org/10.15376/biores.9.3.5208-5218
41. Feuchtegehalt eines Stückes Schnittholz. Teil 1: Bestimmung durch Darrverfahren. (EN 13183-1:2002 + AC:2003) (Moisture content of a piece of sawn timber - Part 1: Determination by oven dry method (EN 13183-1:2002 + AC:2003)), ÖNORM EN 13183-1, Österreichisches Normungsinstitut, 2004 (in German)
42. Plättchen-Biegeversuch für metallische Werkstoffe (Plate bending test for metallic materials), VDA 238-100, Verband der Automobilindustrie E. V. (VDA), 2017
43. F. Mendoza-Santoyo, M. de la Torre-Ibarra, M. del Socorro Hernández-Montes, J.M. Flores Moreno, and B. Pang, *Digital Image Correlation, Full Field Optical Metrology and Applications*, IOP Publishing, Bristol, 2022
44. Livermore Software Technology (LST) Corporation, LS-Dyna R13.0 Keywords user's manual, volume II, Material Models; 09/27/21 (r:14196) LS-DYNA R13; LST Troy, MI, USA, 2021
45. T. Wang, Y. Wang, R. Crocetti, and M. Wålinder, Influence of Face Grain Angle, Size, and Moisture Content on the Edgewise Bending Strength and Stiffness of Birch Plywood, *Mater. Des.*, 2022, **223**, p 111227. https://doi.org/10.1016/j.matdes.2022.111227
46. P. H. Sulzberger, The Effect of Temperature On The Strength Of Wood, Plywood And Glued Joints, Ph.D. Dissertation, University of Tasmania, Hobart TAS, Australia, 1955
47. S. Ebnesajjad, *Adhesives Technology Handbook*, 2nd ed. William Andrew Inc., Norwich, 2008, ISBN 978-081-551-601-9
48. L. Salmén and I. Burgert, Cell wall features with regard to mechanical performance. A review. COST Action E35 2004–2008: wood machining—micromechanics and fracture, *Holzforschung*, 2009, **63**(2), p 121–129. https://doi.org/10.1515/HF.2009.011
49. H.J. Blaß and C. Sandhaas, *Timber Engineering. Principles for Design*, KIT Scientific Publishing, Karlsruhe, 2017, p 37–44, ISBN 978-3-7315-0673-7
50. A.J. Panshin and C. de Zeeuw, *Textbook of Wood Technology: Structure, identification, properties, and uses of the commercial wood of the United States and Canada*, 4th ed. McGraw-Hill Book Co., New York, NY, USA, 1980
51. C.S.P. Borges, E.A.S. Marques, R.J.C. Carbas, C. Ueffing, P. Weißgraeber, and L.F.M.D. Silva, Review on the Effect of Moisture and Contamination on the Interfacial Properties of Adhesive Joints, *Proc. Inst. Mech. Eng. Part C J. Mech. Eng. Sci.*, 2021, **235**(3), p 527–549. https://doi.org/10.1177/0954406220944208